Additive Manufacturing 37 (2021) 101694

Contents lists available at ScienceDirect

Additive Manufacturing

journal homepage: www.elsevier.com/locate/addma

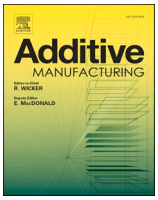

Research Paper

Self-terminating etching process for automated support removal and surface finishing of additively manufactured Ti-6Al-4 V

Subbarao Raikar, Meredith Heilig, Avinash Mamidanna, Owen J. Hildreth *

Colorado School of Mines, Department of Mechanical Engineering, 1500 Illinois St., Golden, CO 80401, USA

ARTICLE INFO

Keywords:
Additive manufacturing
Powder bed fusion
Ti-6Al-4V
Dissolvable supports
3D printing

ABSTRACT

The advent of Additive Manufacturing (AM) has widened the design space for Ti-6Al-4 V (Ti64) components. However, the complex geometries fabricated using AM can result in high post-processing costs due to challenges associated with support removal, powder removal, and improving surface finish. To address these issues, this work introduces a novel, self-terminating etching process for Ti64 alloys that can remove support structures and trapped powder while also improving surface finish for both exterior and interior features. The component is first treated in a furnace to sulfidize the outer 50–150 μm of its surface and the supports. Next, this sulfide layer is selectively dissolved in a solution of 5 M H_2SO_4 and 0.25 M Na_2MoO_4. This solution readily dissolves sulfides without dissolving the Ti64 base metal and enables this etching process to be uniquely self-terminating at the sulfide/Ti64 interface. For this work, the amount of Ti64 converted to sulfides as a function of sulfidation temperature, the surface roughness before and after each sulfidation-dissolution cycle, and the microstructural evolution was quantified. The inherently self-terminating nature of this novel process means that, for the first time, post-processing of Ti64 components can be done in a geometry agnostic manner with the knowledge that a specified and known amount of material will be removed from all surfaces. As a result, support structures and trapped powder can be removed with ease at the same time that the surface finish is improved. This process is expected to reduce post-processing costs while expanding the design space for additively manufactured Ti64 parts.

1. Introduction

Ti-6Al-4 V alloy (Ti64) is a binary-phase titanium alloy with high strength-to-weight ratio, high fracture toughness, excellent corrosion resistance [1], and superior biocompatibility [2–4]. Due to these combined properties, Ti64 is widely used in the aerospace, marine, automobile, chemical, and biomedical industries [3]. Unfortunately, conventional manufacturing processes, such as casting, milling, and forging, have long lead-times and are expensive. Recent advances in Powder Bed Fusion (PBF) Additive Manufacturing (AM) of Ti64 address many of the shortcomings of conventional manufacturing techniques by enabling a cost-effective design space for the production of complex geometries with low material waste and shorter lead time [5,6]. While AM Ti64 has numerous manufacturing benefits, the resulting components often require extensive post-processing to remove support structures [7,8], remove the trapped powder [9,10], and smooth surfaces [11,12]. This results in added costs and can hinder the design freedoms that AM is supposed to enable [13].

To reduce the post-processing burden of PBF AM techniques, Lefky et al. recently introduced a novel self-terminating etching process that can easily dissolve supports and trapped powder while also improving surface finish for PBF AM stainless steel alloys (types 316 and 17–4 PH [14] and PBF AM nickel-based superalloy Inconel 718 [15]. This technique uses a sensitization process to reduce the corrosion resistance of the outer 100–200 μm of the material, creating a hard etch stop between the base component metal and the sensitized region. Since most supports and trapped powder agglomerations are less than 300 μm wide, they can be fully sensitized and dissolved in a self-terminating manner while the component loses a uniform amount of material (100–200 μm) from all surfaces. The sensitization process begins by immersing the component in a saturated aqueous solution of sodium hexacyanoferrate (II) decahydrate, this leaves behind a layer of sodium hexacyanoferrate (II) decahydrate salt over all surfaces. Next, the component heat treated (typically following a heat treatment schedule similar to the ones used to remove residual stresses and refine the microstructure of AM parts) in an inert or reducing atmosphere (by adding excess carbon around the part).

* Corresponding author.
E-mail address: ohildreth@mines.edu (O.J. Hildreth).

https://doi.org/10.1016/j.addma.2020.101694
Received 12 June 2020; Received in revised form 31 October 2020; Accepted 2 November 2020
Available online 7 November 2020

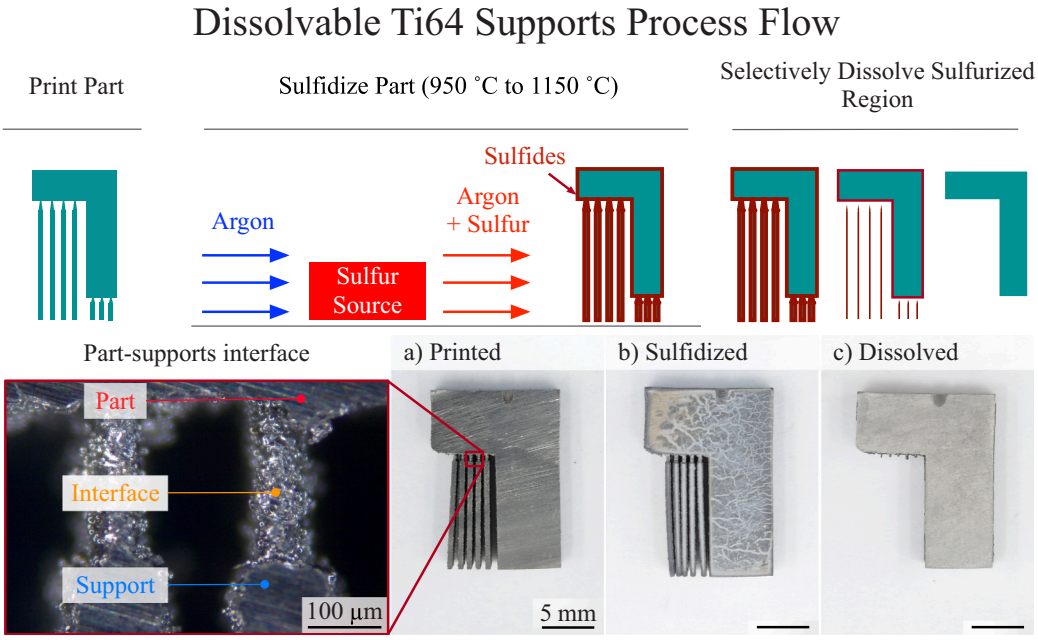

Fig. 1. Schematic of the dissolvable supports process for Ti64 with an example of PBF-printed Ti64 part. The part with supports is sulfurized in a furnace. Sulfur reacts with the top 50–100 µm of the part and the supports, forming sulfides. The sulfurized supports and the top 50–100 µm of the part are selectively dissolved in a solution of H_2SO_4 and Na_2MoO_4.

At the temperatures used, the sodium hexacyanoferrate (II) decahydrate decomposes and leaves behind a layer of carbon on the surface that diffuses into the top 100–200 µm of the part. This carbon combines with the passivating element chromium in these alloys to form inert carbides and reduces the corrosion resistance within this "sensitized region" [15]. The thin supports, trapped powder, and the majority of the surface defects can be completely sensitized in this step. Next, the sensitized part is immersed in a solution of HNO_3 and KCl and dissolved under a bias such that the sensitized layer is anodically dissolved while the base metal is cathodically protected. The net result is a self-terminating etching process that can selectively remove support structures and trapped powder while improving surface finish that maintains the overall geometry of the component.

While carbon sensitizes many chromium-rich alloys, such as stainless steel and nickel super alloys (e.g. Inconel), it would not work for alloys that are inherently self-passivating – such as aluminum or titanium alloys. Using Ti64 as an example alloy, this work addresses this limitation by introducing a new sulfur-based surface treatment that form soluble sulfides. The schematic and example component in Fig. 1 illustrates the overall process. These sulfides can then be selectively dissolved using either chemical or electrochemical methods. For this work, the sulfides were chemically dissolved in a solution of H_2SO_4 with Na_2MoO_4 added to passivate the underlying Ti64 metal. Along with demonstrating the ability of this process to remove supports from complex geometries, this manuscript reports the sulfide thickness and Ti64 consumption thickness as a function of temperature, the resulting Ti64 microstructure, and the R_a roughness showing about a 10× reduction in R_a surface roughness. The process detailed in this manuscript could be directly integrated with the stress relief and microstructure refinement heat treatment with and an entire build platform's worth of components processed in parallel. In summary, a novel approach to self-terminating support removal is demonstrated with the potential for decreasing costs and further expanding the design space for additively manufactured Ti-6Al-4 V parts.

2. Materials and methods

2.1. Sample fabrication

Ti-6Al-4 V (Ti64) discs (16 mm diameter, 5 mm thick) were fabricated using an EOS M290 printer. The discs were fabricated using the following processing conditions: 30 µm layer thickness with laser power of 280 W, speed of 1200 mm/s, and hatch spacing of 0.14 mm. The composition of the Ti64 powder as stated by the powder manufacturer (EOS) was Al: 5.50–6.75 wt%; V: 3.50–4.50 wt%; O: $\leq$ 0.2 wt%; N: $\leq$ 0.05 wt%; C: $\leq$ 0.08 wt%; H: $\leq$ 0.015 wt%; Fe: $\leq$ 0.30 wt%; Y: $\leq$ 0.005 wt%; other elements: $\leq$ 0.4 wt%; and Ti: balance. The discs were printed with the circular faces perpendicular to the printer bed and the build direction. The build-orientation of the discs was noted, and a small cut was made into the build direction using a small Dremel so that roughness scans before and after treatment could be consistently oriented. After marking, the discs were cleaned in an ultrasonic bath with deionized (DI) water (18.2 MΩ, Thermo Scientific Smart2Pure) and followed by isopropyl alcohol for 5 min each. The excessive isopropyl alcohol on the surface of the discs was removed using a flowing stream of compressed N_2. Prior to sulfidation, sample mass and dimensions were measured using XS105 Mettler Toledo mass balance with 0.01 mg precision, Fowler calipers, and an S112XTB Mitutoyo variance indicator.

2.2. Sulfidation treatment

All samples were sulfurized in a tube furnace (Lindberg HT55342C) equipped with a mullite tube (50.8 mm outer diameter, 44.4 mm inner diameter, 1.4 m long). The temperature profile of the heated tube was measured at each sulfidation temperature using a thermocouple (OMEGACLAD XL, Omega). The Ar inert carrier gas (99.999%, General Air) was purified using a titanium-based inert gas purifier (Model GP-100, RD Mathis) and its O_2 levels monitored using an electrochemical cell (Model 2001LC - T2, Advanced Micro Instruments); typical O_2 levels were less than 1 ppm. Vapor-phase elemental sulfur carried by Ar was generated by filling an alumina boat with 20 g of sulfur flakes ($\geq$99.99% trace metals basis, Sigma-Aldrich) located within the 150 °C region of the tube furnace (as estimated from the temperature profiles). Samples

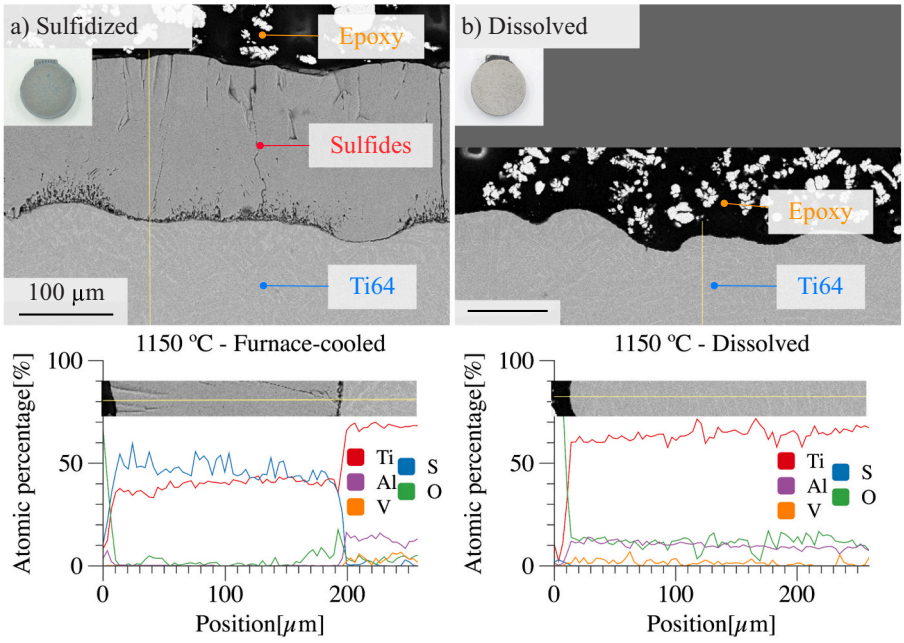

Fig. 2. SEM image showing the cross-section of a) the sulfurized region formed after a 4-hour sulfidation cycle at 1150 °C and b) the disc with dissolved sulfurized region after a dissolution cycle in a solution of 5 M H_2SO_4 and 0.25 M Na_2MoO_4, with the respective EDS line-scan data showing the atomic elemental composition. Inset images: Top view image of the discs (a) after sulfidation and (b) after dissolution showing the discoloration of the disc after sulfidation and the absence of the discolored layer after dissolution.

were loaded upright in an alumina boat (see Fig. S1 in Supporting Information) and placed in the center of the furnace with one of the print-sides (the leading circular face) facing the carrier gas.

After loading the sulfur and samples, the tube was purged with the purified Ar for 2 h at 0.45 standard liters per minute (SPLM) with a gauge pressure of 0.55 bar (8 psig) to clear the tube of any trapped air. The process flow is illustrated in Fig. 1. Positive pressure and flow were maintained during sulfidation to reduce oxygen ingress. After the 2-hour Ar purge, the furnace was heated to between 950 °C to 1150 °C at 10 °C/min and then held there for 4 h. After 4 h, samples were either furnace cooled to room temperature or quenched in an ice-water bath. Next, the sulfurized samples were removed from the furnace and their masses were measured. The delicate nature of the brittle sulfide films prohibited measuring the sample height and diameter using mechanical calipers.

2.3. Sulfide dissolution

Sulfurized samples were cleaned with deionized water in an ultrasonic bath for 5 min and the excess water was removed with compressed N_2. An electrolyte solution was prepared by mixing sulfuric acid (H_2SO_4, 95–98%; VWR Chemicals), deionized water (18 MΩ, Thermo Scientific Smart2Pure), and sodium molybdate (Na_2MoO_4, Sigma-Aldrich) to a final concentration of 5 M H_2SO_4 and 0.25 M Na_2MoO_4. The Na_2MoO_4 is a strong oxidizing agent often used to inhibit Ti64 corrosion in H_2SO_4 [16]. The sulfurized samples were submersed in 250 mL of the electrolyte solution while the solution was stirred using a stir station and sonicated in an ultrasonic bath. The electrolyte solution was replaced after it turns very dark (as shown in Fig. S2 in the Supporting Information), typically after 15 h; further investigation is necessary to identify the ideal time to replace the solution. The samples were cleaned with deionized water in an ultrasonic bath every time the electrolyte solution was replaced and after the end of the dissolution process.

2.4. Metrology

To gather cross-section data (composition and microstructure), the samples were preserved in a two-step mounting process. Each sample was placed with the leading circular face up in a mixture of copper powder (Allied High-tech) and cold-curing epoxy (EpoFix, Struers) within 1-inch diameter mold cups (Allied High-tech). The fully cured 1-inch mounts cross-sectioned using a metallographic saw (LECO MSX-250 M2) with an Al_2O_3 abrasive blade and then fixed with the cut face down in epoxy only in 1.25-inch diameter mold cups. This two-step sample preparation process was used to prevent the fragile sulfide films from breaking off during cutting and copper powder was added in the first step to enable better edge detection during Scanning Electron Microscopy (SEM) and Energy Dispersive Spectroscopy (EDS). The double mounted, cross-sectioned samples are prepared with sequentially finer media starting with silicon carbide paper ranging from 180 grit to 600 grit, moving to 9 µm diamond suspension, and finishing with 0.05 µm colloidal silica, and thoroughly rinsed and dried between each step. For microstructural analysis, samples were stain etched at room temperature using an immersion solution of ammonium bifluoride and deionized water for 60 s. Light optical microscopy (Zeiss Axio Vert.A1) was used for microstructural examination. Digital photography (Nikon D7000 and Nikon D3300) was used to document the sample evolution throughout the sample preparation process. Scanning Electron Micrographs (SEM) were taken using the top-down Backscattered Secondary Electron (BSE) detector of TESCAN MIRA3 SEM at 20 kV accelerating voltage with a 10 mm working distance. The BSE detector was used because it provides increased elemental contrast as compared to the secondary electron detector. Elemental composition data (line scans and maps) were collected using a Bruker XFlash 6|30 EDXS detector at 20 kV. X-Ray Diffraction (XRD) patterns were collected from the leading circular surfaces of the samples before sulfidation, after sulfidation, and after sulfide dissolution using a Malvern-PANalytical Empyrean system with a Cu source, Bragg-Brentano mirror, and a Galipax digital detector. This XRD data was used for phase identification and phase distribution quantification. Surface roughness was quantified using a Bruker DektakXT contact profilometer using a 2 µm stylus tip radius with 1 mm scan lengths at 2000 µm/min. The scans were 3.5 mm on both the sides of the center and at the center on the flat surface of the discs as shown in the inset Fig. 5. The roughness parameters were recalculated in accordance with ISO 4287 standard with a long cut-off wavelength (λ_c) of 0.25 mm and a short cut-off wavelength (λ_s) of 2.5 µm [17]. The cut-off wavelengths were chosen based on the mean width of profile elements (RSM) of 0.12 mm. The evaluation length is 0.25 mm lesser than the recommended evaluation length of 1.25 mm. However, this is maintained consistent for all the samples evaluated. The profiles were levelled using a linear fit.

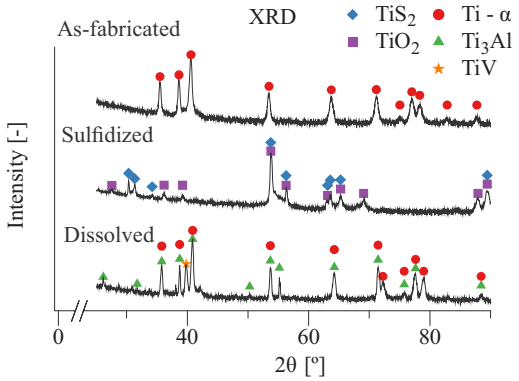

Fig. 3. XRD of the a) as-fabricated Ti64 disc showing the presence of alpha and beta phases, b) sulfurized disc confirming the formation of TiS_2 and TiO_2, and c) dissolved disc showing only the Ti-α and Ti-β peaks, indicating that the dissolution of the sulfide layer in a solution of 5 M H_2SO_4 and Na_2MoO_4 removes both the TiS_2 and TiO_2. See Figs. S4–S6 for individual, detailed graphs.

3. Results and discussion

3.1. Proof-of-concept

The self-terminating etching process detailed in this work is divided into two steps: the sulfidation step, to change the composition of the surface; the subsequent etching step to remove the sulfides. This cycle might need to be repeated depending on how much Ti64 is consumed during the sulfidation step. For this work, elemental sulfur was chosen as the sulfurizing agent over H_2S to avoid the complications of dealing with the high toxicity of H_2S. A solution of H_2SO_4 and Na_2MoO_4 was selected as an etching solution. This etchant was selected by first conducting a small study, comparing the ability of HCl, HNO_3, and H_2SO_4 to dissolve the sulfide films formed on Ti64 substrates. For this initial study, sulfurized samples were immersed overnight in the concentrated acid solutions: 8 M HCl, 2 M HNO_3, and 4.5 M H_2SO_4. H_2SO_4 readily removed the surface sulfides; however, H_2SO_4 is a reducing acid that also dissolves Ti64 [16]. Adding Na_2MoO_4, a common corrosion inhibitor for Ti64 metal alloys [16], blocks the dissolution of Ti64 while allowing the sulfides to be dissolved, albeit at a slower rate. Both untreated and sulfurized samples cut from an extruded rod of Ti64 (TMS Titanium) were placed in solutions of 5 M H_2SO_4 and 0.125 M, 0.25 M, and 0.5 M of Na_2MoO_4 for 20 h. Based on the recorded amounts of Ti64 removed in each solution (see Supporting Information Fig. S3), a final etchant solution of 5 M H_2SO_4 and 0.25 M Na_2MoO_4 was chosen for these studies.

Fig. 2a illustrates the process with an SEM image of the cross section of a disc sulfurized at 1150 °C for 4 h. A distinctive region above the Ti64 region shows the formation of a sulfide layer and the EDS line-scan along the cross section shows a high concentration of sulfur (~ 50 at%) for a sulfide layer thickness of about 200 μm. The sharp drop in the sulfur concentration across the two regions, indicates that the transition from the region of high dissolution susceptibility to a region of low dissolution susceptibility occurs over a depth of less than 10 μm. The SEM image of the cross section of a previously sulfurized disc immersed in a solution of 5 M H_2SO_4 and 0.25 M Na_2MoO_4 in Fig. 2b indicates the absence of the sulfide layer after the dissolution process. A sulfur signal is absent in the EDS line-scan along the cross section, indicating that the sulfide layer has been completely removed. This is a big difference compared to the carbon-based approach Lefky et al. used for stainless steel and Inconel 718, where the etch-stop location across the sensitized region can be changed by changing the applied potential [18]. We currently attribute this difference to the fact that the diffusion kinetics of carbon-based sensitization in ferrous alloys is defined by the diffusion of carbon inward, followed by carbide formation [15]. In contrast, diffusion kinetics of sulfidation in titanium ternary alloys are largely driven by the diffusion of metal outward through the sulfide layer [19]. As a result, there is a sharp transition from the base metal alloy to the sulfide film.

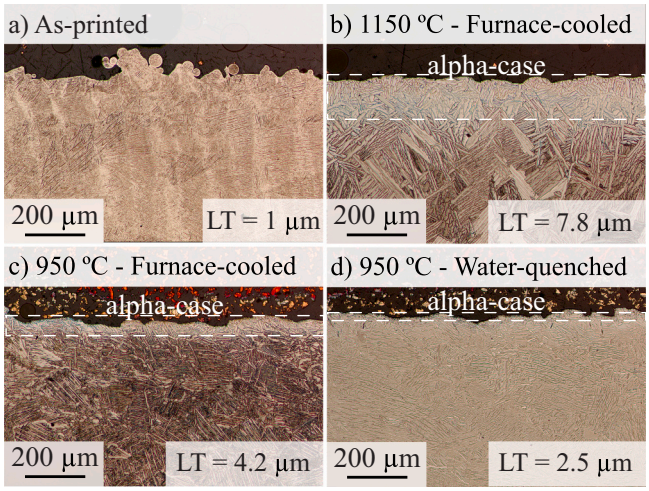

Fig. 4. Optical images of the cross-section of the discs tint-etched with ammonium bifluoride - a) as-printed b) sulfurized at 1150 °C c) sulfurized at 950 °C and d) sulfurized at 950 °C and quenched in water. The α-lath thicknesses (LT, mentioned in the right bottom corner all the images) were measured to be 1 μm for as-printed, 7.8 μm for 1150 °C furnace-cooled disc, 4.2 μm for 950 °C furnace-cooled disc, and 2.5 μm for 950 °C quenched disc. Note, the red/orange color is from the copper particles embedded in the mounting epoxy.

The successful sulfidation and dissolution are further corroborated with XRD spectra acquired from the Ti64 samples shown in Fig. 3. Fig. 3a is the diffractogram of the as-printed disc before sulfidation showing only the Ti-α and Ti-β peaks. The diffractogram from the disc surface after sulfidation (Fig. 3b) shows titanium disulfide (TiS_2) and titanium dioxide (TiO_2) peaks; this indicates TiS_2 and TiO_2 form during the sulfidation process. The formation of TiO_2 can be attributed to a mixture of trace oxygen within the Ar carrier gas, possible O_2 absorption into the sulfur source, possible ingress from the atmosphere, and degassing of the mullite tube and the alumina boat in the furnace. TiO_2 formation is undesirable due to its extremely high stability and corrosion resistance. However, we suspect that the TiO_2 is distributed in a matrix of TiS_2; when TiS_2 dissolves TiO_2 is not structurally supported which leads its successful removal. Fig. 3c is the diffractogram of the disc after sulfide dissolution. The absence of the TiS_2 and TiO_2 peaks in Fig. 3c confirms the complete dissolution of the sulfide layer corroborating the EDS data. See Fig. S4 – Fig. S6 in the Supporting Information for individual, detailed graphs.

3.2. Effect on the microstructure

From the above-discussed results, Ti64 is shown to be successfully sulfurized and dissolved using an overly aggressive heat treatment designed to test the overall concept. It is known that at temperatures above 1050 °C [20], Ti64 grains grow rapidly, which is detrimental to its mechanical properties. Therefore, two temperatures of 950 °C and 1150 °C were chosen for the heat treatment studies. 950 °C is below the temperature where α-laths grow significantly while 1150 °C is above that transition temperature. In addition, at 950 °C, a faster cooling method (water-quenching) was studied with a goal to further curb the growth of the α-laths. Fig. 4 compares the Ti64 microstructure of samples in the as-printed/as-received condition and samples after sulfidation and dissolution for (a) as-printed samples; (b) furnace cooled after 4 h at 1150 °C; (c) furnace-cooled after 4 h at 950 °C; (d) water-quenched after 4 h at 950 °C. As expected, significant grain growth is observed in the disc sulfurized at 1150 °C in which the average α-lath thickness increased from 1 μm in the as-printed disc to 7.8 μm

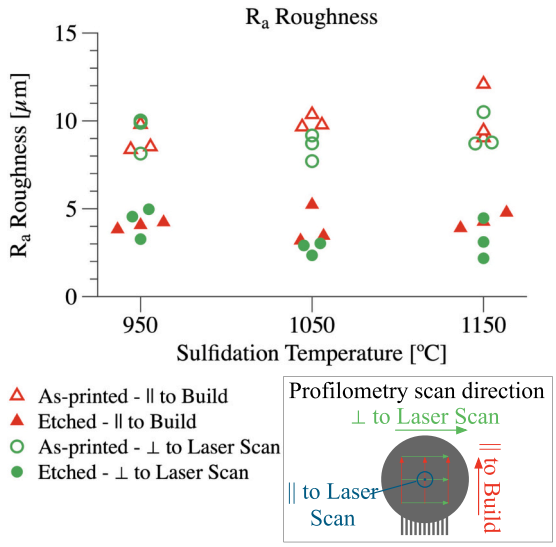

Fig. 5. Plot of the surface roughness of the discs before and after dissolution against different sulfidation temperatures showing the decrease in surface roughness by at least half the surface roughness of the as-printed disc.

after sulfidation as shown in Fig. 4a and b. For the furnace-cooled, 950 °C sample, the average α-lath thickness (LT) is 4.2 μm and a significant decrease in the α-case thickness is observed. For the water-quenched, 950 °C sample, the average α-lath thickness is 2.5 μm which is significantly narrower than that at 1150 °C and comparable to the as-printed microstructure. The α-case layer is detrimental to mechanical properties and is commonly removed from Ti64 castings by chemical milling with the use of hydrofluoric acid [21]. The formation of a thick alpha-case region is observed in the disc sulfurized at 1150 °C as shown in Fig. 4b. The thickness of alpha-case decreases as the temperature is reduced from 1150 °C to 950 °C, and it further decreases on water-quenching. The microstructure observed with disc sulfurized at 950 °C and water-quenched is the closest to the one observed with the as-printed disc. Sulfidation at 950 °C followed with water-quenching achieves a microstructure closest to that which is observed in the as-printed disc. Additionally, 950 °C also aligns with the commonly employed solution treatment temperature to produce maximum strength in titanium alpha-beta alloys [22], so this temperature was used for the rest of this work. It is important to note, the part can always be subjected to additional solution treatment and rapid quenching to obtain finer microstructure as long as alpha-case formation is avoided.

3.3. Effect on the surface roughness

Surface roughness is an important parameter that affects mechanical performance, including fatigue performance [23]. AM components are known to have higher surface roughness than many conventional manufacturing techniques [24] and this surface roughness needs to be reduced to improve fatigue performance. In order to study the impact of a sulfidation-etching cycle, four types of surface roughness data (R_a – average roughness; R_q – root mean square deviation of the profile; R_p – maximum measured profile peak; R_v – maximum measured valley depth; R_z – average height difference between the peaks and valleys; and R_t – distance between the maximum peak and the maximum valley) were collected using contact profilometry with three scans parallel to the build direction and the other three perpendicular to the laser scan direction (see inset in Fig. 5). Fig. 5 plots the R_a roughness at each sulfidation temperature after a single sulfidation/dissolution cycle in comparison to that measured in as-printed samples (See Fig. S9 in the Supporting Information for the other roughness values). Interestingly and favorably, the roughness of the discs after one sulfidation/etching cycle reduced by at least half for all samples. However, there is no conclusive trend in surface roughness across discs sulfurized at different temperatures.

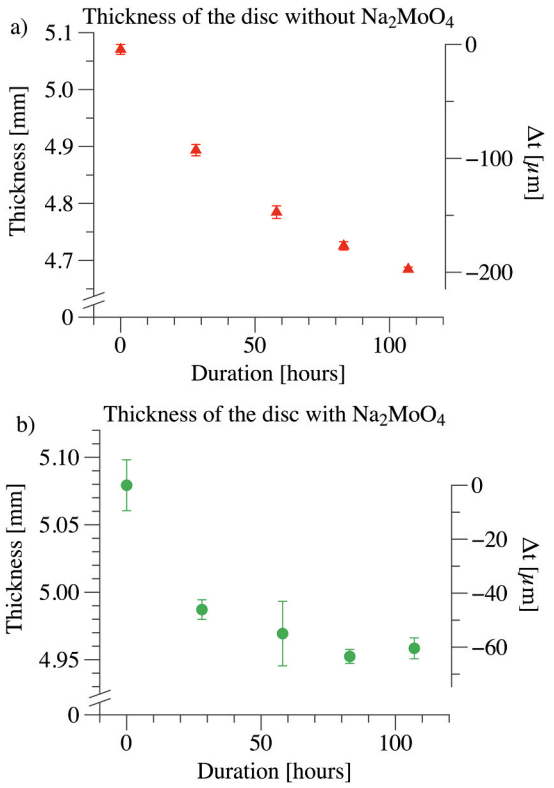

Fig. 6. Plot of the thickness of the disc a) dissolved in 5 M H_2SO_4 without any Na_2MoO_4 and b) dissolved in a solution of 0.25 M Na_2MoO_4 and 5 M H_2SO_4. The thickness of the disc in the electrolyte with Na_2MoO_4 does not vary after 80 h of etching, showing the self-termination attribute of the dissolution process. The axis on the right shows the amount of Ti64 removed from the surface of the disc in μm.

3.4. Self-termination aspect of the process

Acids have been used to etch/dissolve metals for hundreds of years [25]. Removal of printed supports can certainly be achieved by immersing a printed part in an acid. However, traditional chemical and electrochemical machining processes are not self-terminating and it can be difficult, or even impossible, to tightly maintain dimensional tolerations for components with complex shapes [26]. This issue is exemplified by etching a sample in 5 M H_2SO_4 without any Na_2MoO_4 corrosion inhibitor. As shown in Fig. 6a, which plots the thickness of the disc and the amount Ti64 removed from the surface (Δt) versus the etch duration, shows that the sulfurized Ti64 samples continually lose material throughout the etching process. The rate of dissolution is fairly linear, and the disc continues to dissolve at the same rate even after 100 h of etching. With the addition of Na_2MoO_4, self-termination is achieved, as shown in Fig. 6b. The change in the thickness of the disc after about 40 h of dissolution represents the dissolution of the sulfide layer. The rate of dissolution for the disc etched in the presence of Na_2MoO_4 reduces with time with no significant change in the thickness of the disc after 80 h of etching. The slight variations in the measurements are attributed to the difference in the location of the measurements using handheld calipers.

The slow etch rate of the sulfide layer is likely due to the presence of TiO_2 formed during the sulfidation process. Preliminary etching studies demonstrated that TiS_2 powder (Sigma Aldrich) readily dissolves in both H_2SO_4 and H_2SO_4-Na_2MoO_4 solution. However, XRD analysis of our

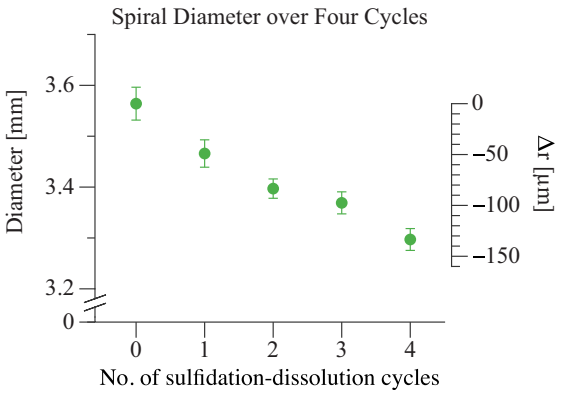

Fig. 7. Plot of the diameter of the printed spiral after each sulfidation-etching cycle. The axis on the right shows the amount of Ti64 removed from the surface of the disc in μm. The part would have to be built oversized to account for the loss of material for functional accuracy.

initial Ti64 samples sulfurized prior to the addition of an O_2 scrubber showed high levels of TiO_2 and large sections of the sulfurized samples would fail to etch. Decreasing the O_2 levels in the Ar carrier increased etch rate and etch completeness. However, some TiO_2 is still observed in the XRD pattern (see Fig. 3) and is likely slowing the etching process. Future work will investigate the role of trace O_2 and TiO_2 on the etching process to decrease the time required for complete dissolution.

3.5. Demonstration of the process on a printed part with supports

Support removal is demonstrated using a two-step process designed based on the previously discussed results. First, a printed part with ~ 200 μm thick supports was sulfurized at 950 °C for 4 h and quenched in a water bath. The resulting sulfide layer was dissolved in 5 M H_2SO_4 and 0.25 M Na_2MoO_4. Each sulfidation-etching cycle at 950 °C removed about 50 μm of Ti64; the process was repeated three times to completely dissolve the supports. The printed part lost 150 μm compared to the 200 μm of the support thickness removed; the change in the diameter of the printed part, measured using calipers, with every cycle has been shown in Fig. 7. The axis on the right shows the change in the radius of

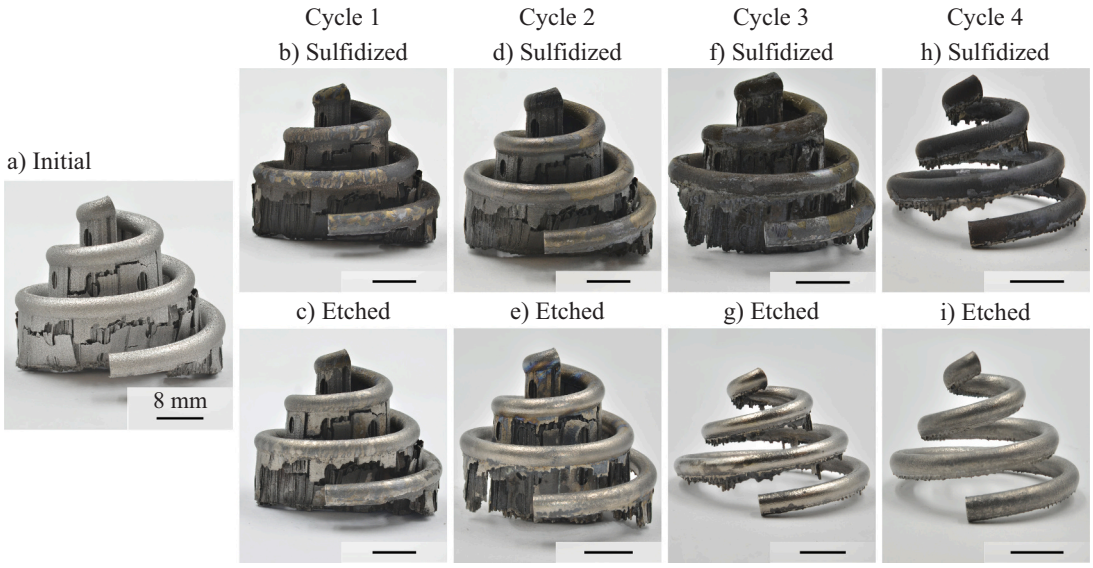

Fig. 8. Optical images of a printed Ti64 part with supports. a) as-printed spring was used to test the sulfidation and dissolution process; b) after the first sulfidation; c) after the first etching cycle; d) after the second sulfidation; e) after the second etching cycle; f) after the third sulfidation; g) after the third etching cycle; h) after the fourth sulfidation; and i) after the fourth etching cycle. The supports get more porous with every cycle and eventually separate from the part.

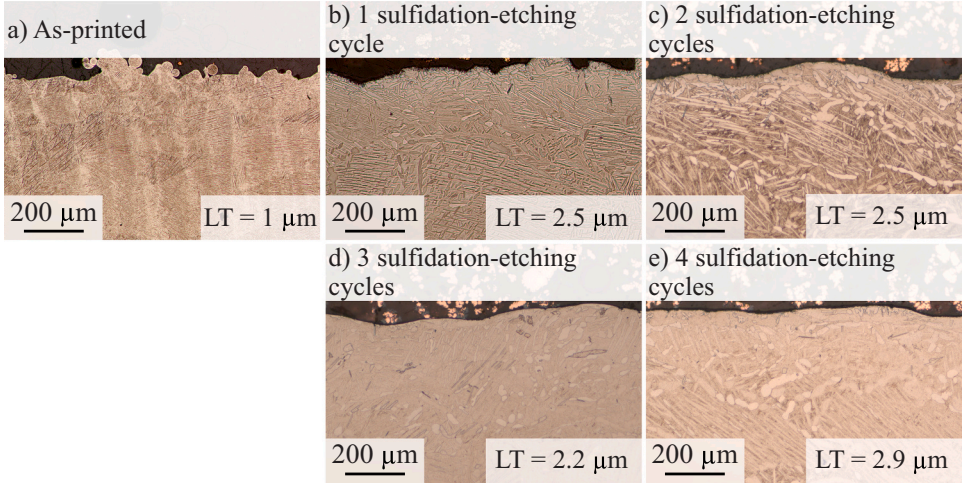

Fig. 9. Optical images of the cross-section of the discs as-printed and that underwent different sulfidation-etching cycle: a) as-printed; b) one sulfidation-etching cycle; c) two sulfidation-etching cycles; d) three sulfidation-etching cycles; and e) four sulfidation-etching cycles. The α-lath thicknesses (LT, mentioned in the right bottom corner all the images) were measured to be 1 μm for as-printed, 2.5 μm after one cycle, 2.5 μm after two cycles, 2.2 μm after three cycles, and 2.9 μm after four cycles. Note, the red/orange color is from the copper particles embedded in the mounting epoxy.

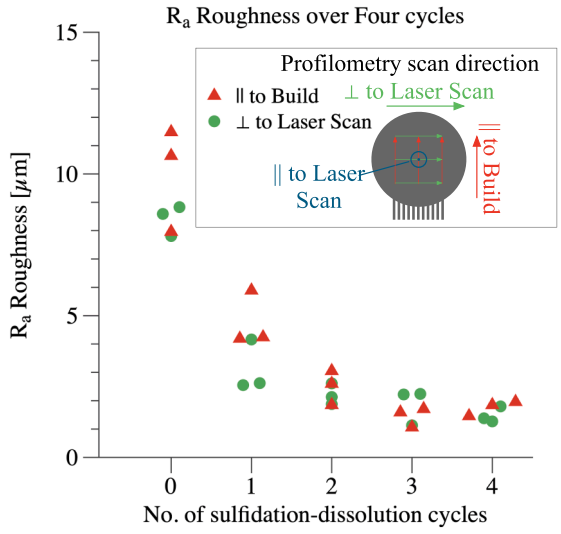

Fig. 10. Plot of the surface roughness R_a of the disc after each sulfidation-etching cycle. The surface roughness improved by 10× from the surface roughness of the as-printed disc.

the spiral after each cycle. The change is radius is a measure of the amount of Ti64 removed from the surface of the spiral. A total of ~ 135 μm of Ti64 was removed from the surface of the spiral and the spiral would have to be built oversized by 135 μm in radius for functional accuracy. The spiral was expected to lose about 50 μm per sulfidation-etching cycle and a total of 200 μm after 4 cycles of sulfidation and etching. The difference in expected and actual amount of Ti64 removed could be due to multiple factors such as the measurement inconsistency, difference in the properties of the printed parts (the discs and the spiral were from different suppliers), and/or the form of the printed parts. Future work will investigate the impact of the above-mentioned factors on sulfidation and etching.

Fig. 8 shows the part throughout the progression of each sulfidation-dissolution cycle. Fig. 8a shows the spiral component with its supports on the bottom. After sulfidation, darkening or discoloration of the part is observed, shown in the upper images: Fig. 8b, Fig. 8d, Fig. 8f, and Fig. 8h. Most of the sulfide layer comes off of the part during the quenching process, shown in the Supporting Information (Fig. S8), due to the residual stresses developed from the large temperature gradient. The lower images: Fig. 8c, Fig. 8e, Fig. 8g, and Fig. 8i show the part after each etching cycle. Visual inspection is used as an indication for the part to be ready for the next sulfidation cycle; when surface discoloration was no longer evident, the part the etching process is stopped. EDS data corroborates the visual inspection process as shown earlier in Fig. 2. Fig. 2a shows the top view of the discolored sulfurized disc along with the EDS line-scan showing that the discoloration has high sulfur content. Fig. 2b shows the top view of the etched disc along with the EDS line-scan showing that the discolored disc has been etched to remove all the sulfurized layer and the top view of the disc shows the removal of the discolored layer.

Four sulfidation-etching cycles removed the supports from the printed Ti64 part. Multiple sulfidation cycles that involve holding Ti64 at an elevated temperature of 950 °C for 4 h, followed by water-quenching can lead to a different microstructure than that obtained from just one sulfidation-etching cycle. Fig. 9 shows the microstructure evolution of the printed discs after the respective number of sulfidation-etching cycles to mimic the sulfidation-etching process of the printed spiral: a) as-printed; b) one sulfidation-etching cycle; c) two sulfidation-etching cycles; d) three sulfidation-etching cycles; and e) four sulfidation-etching cycles. As noted earlier, the microstructure obtained after the one sulfidation-etching cycle (Fig. 9b) is the closest to the as-printed microstructure (Fig. 9a) with the α-lath thickness of 2.5 μm. There is no significant change in the α-lath thickness with multiple-sulfidation-etching cycles. The average α-lath thicknesses are 2.5 μm, 2.2 μm, and 2.9 μm in the discs which underwent two, three, and four sulfidation-etching cycles, respectively. However, the formation of primary-α phase along the prior-β grain boundaries is observed after two sulfidation-etching cycles (Fig. 9b). The primary-α phase along the prior-β grain boundaries appears to be more defined after three and four sulfidation-etching cycles (Fig. 9d and Fig. 9e, respectively). See Supporting Information Fig. S11 for support removal demonstration of another part.

Fig. 9 shows that the cross-sectional edge gets smoother with increased sulfidation-etching cycles. Profilometry scanning of the surface of the disc, which underwent four sulfidation-cycles after each sulfidation-etching cycle, shows that the R_a roughness of the disc undergoes a ten-fold decrease from a high of 11 μm to a low of 1 μm. The R_a roughness decreases and becomes more uniform with each successive sulfidation-etching cycle (Fig. 10). (See Fig. S9 in the Supporting Information for the other roughness values). The marked decrease in R_a roughness after two sulfidation-etching cycles is attributed to the removal of the surface irregularities, as seen in Fig. 9a and Fig. 9b. Every sulfidation-etching cycle after the second cycle helps with the reduction of the surface waviness, as seen in Fig. 9c and Fig. 9d.

To further improve this process, future work will look into characterizing the sulfidation rate as a function of temperature and sulfur concentration to provide better control over sulfidation depth, microstructure evolution, surface roughness, and process uniformity for complex parts. Additionally, it would be advantageous to evaluate the effectiveness of colloidal pastes as a means of "masking" regions from sulfidation and etching.

4. Conclusions

In conclusion, we demonstrated a novel approach for selectively dissolving the support structures in a Ti64 part printed using PBF. This process can be very easily integrated into the current industry setup since it is independent of the printing process parameters. This unique approach simplifies the support removal process in metal AM by reducing the reliance on labor-intensive, time-consuming, and expensive processes, even when the supports are mechanically inaccessible. The applicability of dissolvable supports technology was explored at temperatures above and below 1050 °C, and the resulting microstructures were studied. Water-quenching was used to obtain a microstructure closest to an as-printed microstructure to ensure the process did not result in untenable microstructural changes. After four sulfidation-etching cycles, the average surface roughness of the printed discs was reduced by about 90% and resulted in primary-α formation along the prior-β grain boundaries. Overall, this research presents the possibility of opening the AM Ti64 design space for more complex and waste-reducing designs.

5. CRediT authorship contribution statement

Subbarao Raikar: Conducted to all experiments, Writing - original draft, Revisions, Data Analysis. **Meredith Heilig:** Experiments and data analysis for microstructure, Writing - review & editing. **Avinash Mamidanna:** Experiments on heat treatment. **Owen Hildreth:** Supervision, Conceptualization, Methodology, Writing - review & editing.

Declaration of Competing Interest

The authors declare that they have no known competing financial interests or personal relationships that could have appeared to influence the work reported in this paper.

Acknowledgment

Hildreth group gratefully acknowledges the support from the United States Department of Energy under contract agreement Grants #: DE-EE0008166 administred through the Department of Energy's Kansas City National Security Campus, operated by Honeywell Federal Manufacturing & Technologies, LLC, under contract number DE-NA0002839. We also acknowledge the support from the United States National Science Foundation (CAREER: 1944516). We acknowledge the support of Christian Barr at the Kansas City National Security Campus for supplying the printed Ti64 discs. The authors would like to express gratitude to Dustin Crouse of 3D Systems for generously supplying the Ti64 spiral.

Appendix A. Supporting information

Supplementary data associated with this article can be found in the online version at doi:10.1016/j.addma.2020.101694.

References

[1] I. Gurrappa, Characterization of titanium alloy Ti-6Al-4V for chemical, marine and industrial applications, Mater. Charact. 51 (2–3) (2003) 131–139, https://doi.org/10.1016/j.matchar.2003.10.006.
[2] M. Long, H.J. Rack, Titanium alloys in total joint replacement—a materials science perspective, Biomaterials 19 (18) (1998) 1621–1639, https://doi.org/10.1016/S0142-9612(97)00146-4.
[3] S. Liu, Y.C. Shin, Additive manufacturing of Ti6Al4V alloy: a review, Mater. Des. 164 (2019), 107552, https://doi.org/10.1016/j.matdes.2018.107552.
[4] H. Attar, S. Ehtemam-Haghighi, N. Soro, D. Kent, M.S. Dargusch, Additive manufacturing of low-cost porous titanium-based composites for biomedical applications: advantages, challenges and opinion for future development, J. Alloy. Compd. 827 (2020), 154263, https://doi.org/10.1016/j.jallcom.2020.154263.
[5] M. Attaran, The rise of 3-D printing: the advantages of additive manufacturing over traditional manufacturing, Bus. Horiz. 60 (5) (2017) 677–688, https://doi.org/10.1016/j.bushor.2017.05.011.
[6] G.T. Haar, T. Becker, Selective laser melting produced Ti-6Al-4V: post-process heat treatments to achieve superior tensile properties, Materials 11 (1) (2018) 146, https://doi.org/10.3390/ma11010146.
[7] S. Nelaturi, M. Behandish, A.M. Mirzendehdel, J. de Kleer, Automatic support removal for additive manufacturing post processing, Comput. Aided Des. 115 (2019) 135–146, https://doi.org/10.1016/j.cad.2019.05.030.
[8] J. Jiang, X. Xu, J. Stringer, Support structures for additive manufacturing: a review, J. Manuf. Mater. Process. 2 (4) (2018) 64, https://doi.org/10.3390/jmmp2040064.
[9] L.W. Hunter, D. Brackett, N. Brierley, J. Yang, M.M. Attallah, Assessment of trapped powder removal and inspection strategies for powder bed fusion techniques, Int. J. Adv. Manuf. Technol. 106 (9–10) (2020) 4521–4532, https://doi.org/10.1007/s00170-020-04930-w.
[10] A. Hussein, L. Hao, C. Yan, R. Everson, P. Young, Advanced lattice support structures for metal additive manufacturing, J. Mater. Process. Technol. 213 (7) (2013) 1019–1026, https://doi.org/10.1016/j.jmatprotec.2013.01.020.
[11] G. Pyka, G. Kerckhofs, I. Papantoniou, M. Speirs, J. Schrooten, M. Wevers, Surface roughness and morphology customization of additive manufactured open porous Ti6Al4V structures, Materials 6 (10) (2013) 4737–4757, https://doi.org/10.3390/ma6104737.
[12] N. Sanaei, A. Fatemi, Analysis of the effect of surface roughness on fatigue performance of powder bed fusion additive manufactured metals, Theor. Appl. Fract. Mech. 108 (2020), 102638, https://doi.org/10.1016/j.tafmec.2020.102638.
[13] G.A.O. Adam, D. Zimmer, Design for additive manufacturing—element transitions and aggregated structures, CIRP J. Manuf. Sci. Technol. 7 (1) (2014) 20–28, https://doi.org/10.1016/j.cirpj.2013.10.001.
[14] C.S. Lefky, B. Zucker, D. Wright, A.R. Nassar, T.W. Simpson, O.J. Hildreth, Dissolvable supports in powder bed fusion-printed stainless steel, 3D Print. Addit. Manuf. 4 (1) (2017) 3–11, https://doi.org/10.1089/3dp.2016.0043.
[15] C.S. Lefky, T.G. Gallmeyer, S. Moorthy, A. Stebner, O.J. Hildreth, Microstructure and corrosion properties of sensitized laser powder bed fusion printed Inconel 718 to dissolve support structures in a self-terminating manner, Addit. Manuf. 27 (2019) 526–532, https://doi.org/10.1016/j.addma.2019.03.020.
[16] T.-P. Cheng, J.-T. Lee, W.-T. Tsai, Passivation of titanium in molybdate-containing sulphuric acid solution, Electrochim. Acta 36 (14) (1991) 2069–2076, https://doi.org/10.1016/0013-4686(91)85211-O.
[17] A. Townsend, N. Senin, L. Blunt, R.K. Leach, J.S. Taylor, Surface texture metrology for metal additive manufacturing: a review, Precis. Eng. 46 (2016) 34–47, https://doi.org/10.1016/j.precisioneng.2016.06.001.
[18] C.S. Lefky, Corrosion and Sensitized Microstructure Evolution of 3D Printed Stainless Steel 316 and Inconel 718 Dissolvable Supports.
[19] H.L. Du, P.K. Datta, D.B. Lewis, Jim S. Burnell-Gray, D. Jenkinson, Oxidation/sulphidation of Ti and Ti-6Al-4V at 750°C alloy, Key Eng. Mater. 99–100 (1995) 151–160, https://doi.org/10.4028/www.scientific.net/KEM.99-100.151.
[20] F.J. Gil, J.A. Planell, Behaviour of normal grain growth kinetics in single phase titanium and titanium alloys, Mater. Sci. Eng. A 283 (1–2) (2000) 17–24, https://doi.org/10.1016/S0921-5093(00)00731-0.
[21] B. Sefer, Oxidation and Alpha-case Phenomena in Titanium Alloys Used in Aerospace Industry: Ti-6Al-2Sn-4Zr-2Mo and Ti-6Al-4V, Luleå University of Technology, Luleå, 2014.
[22] M.J. Donachie, Titanium: A Technical Guide, second edition,, ASM International, Materials Park, OH, 2000.
[23] D. Greitemeier, C. Dalle Donne, F. Syassen, J. Eufinger, T. Melz, Effect of surface roughness on fatigue performance of additive manufactured Ti–6Al–4V, Mater. Sci. Technol. 32 (7) (2016) 629–634, https://doi.org/10.1179/1743284715Y.0000000053.
[24] Pan Wang, Wai Sin, Mui Nai, Jun Wei, Effects of processing parameters on surface roughness of additive manufactured Ti-6Al-4V via electron beam melting, Materials 10 (10) (2017) 1121, https://doi.org/10.3390/ma10101121.
[25] J.N. Bronsted, N.L.R Kane, On the dissolution of metals in acids, J. Am. Chem. Soc. 53 (10) (1931) 3624–3644.
[26] Y. Yuan, L. Han, D. Huang, J.J. Su, Z.Q. Tian, Z.W. Tian, D. Zhan, Electrochemical micromachining under mechanical motion mode, Electrochim. Acta 183 (2015) 3–7, https://doi.org/10.1016/j.electacta.2015.04.046.